Spinal Cord (1998) 36, 531–540

http://www.stockton-press.co.uk/sc

Scientific Review Article

Computer modelling of spinal cord stimulation and its contribution to therapeutic efficacy

Jan Holsheimer

Institute for Biomedical Technology, Department of Electrical Engineering, University of Twente, P.O. Box 217, 7500 AE Enschede, The Netherlands

An overview of computer models developed since the late seventies, which enable the simulation of the primary effects of spinal cord stimulation (SCS) on nerve fibres, is presented. These models consist of a 3-dimensional volume conductor model, representing anatomical structures and their electrical conductivities, and cable models representing the electrical behaviour of nerve fibres. The characteristics of these models and their relation to anatomy and physiology, as well as the calculation of stimulation-induced electrical fields and their effect on nerve fibre models, are reviewed. It is shown that most characteristics of SCS as predicted by computer modelling correspond well with empirical data. Accordingly, a theoretical framework describing the relations between relevant parameters in SCS is presented. Finally, it is shown how theory and computer modeling are applied to improve the efficacy of SCS by the optimization of its technique, primarily by the design of new epidural electrodes.

Keywords: computer modelling; dorsal column stimulation; dorsal root stimulation; epidural electrode; spinal cord stimulation

Introduction

Spinal cord stimulation (SCS) is a therapeutic method applied in a variety of indications, such as chronic neurogenic pain, peripheral vascular disease (PVD), angina pectoris, ischaemic pain related to PVD and angina, and various motor disorders (eg spasticity, dystonia, torticollis, neurogenic bladder).[1–3] The method is based on the 'gate-control' theory of pain and was first applied in 1966 by Shealy *et al*[4] for pain management in a cancer patient. The theory, presented in 1965 by Melzack and Wall,[5] postulates that activity in large calibre cutaneous fibres (Aβ) inhibits (pre)synaptically those neurons in the dorsal horns which transmit noxious information. Electrical stimulation of these large primary afferents by an electrode placed in the dorsal epidural space elicits a tingling sensation (paraesthesia) in the corresponding dermatomes. It is generally accepted that for a successful treatment of chronic, intractable pain the stimulation-induced paraesthesia has to cover the painful area completely.[1–3] Chronic pain management, especially of the low back, is still a major application of SCS.[3]

In three decades SCS systems have evolved from a unipolar electrode powered by a simple pulse generator to both fully implantable, battery powered, programmable single channel pulse generators and radio-frequency controlled, single and dual channel pulse generators, selectably connected to one or two multi-contact epidural electrodes in various anode-cathode combinations (uni/bi/tri/quadrupolar).[2,6] As it appeared rather difficult to obtain a sufficient paraesthesia coverage of the painful area in many chronic pain patients by a uni-bipolar electrode, it was argued that a multitude of electrode contacts distributed over a spinal length of several centimetres would increase the probability of obtaining an adequate combination for each patient empirically. These considerations led to the design of epidural electrodes, both percutaneous (cylindrical) and surgical (plate) ones, holding a rostrocaudal array of four or eight contacts with a centre separation of 7–10 mm or more.[2]

From the beginning of SCS it has been assumed that primarily the dorsal columns (DCs) were stimulated, as expressed by the terminology used in many papers ('Dorsal Column stimulation'). Because the DCs are the neural structure closest to a midline epidural electrode, it was supposed that nerve fibres in this structure would be affected most by the stimulation-induced electrical field.[7]

From a neuroanatomical point of view a discrepancy exists between the assumed 'DC stimulation' and the need to stimulate at various spinal levels and

Correspondence: J Holsheimer

with a multitude of anode-cathode combinations. At any spinal level all dermatomes corresponding to that level and caudally are represented in the DCs in a topological order by their large cutaneous afferents.[8] Theoretically, an electrode position at the radiological midline just cephalad to the spinal segment corresponding to the most rostral (bilateral) painful area would therefore be optimal, while in unilateral pain the electrode could be slightly off midline at the corresponding side.[9,10] Because adequate SCS appeared not to be so simple, and since understanding of the origin(s) of the discrepancy between theory and clinical practice was lacking, SCS continued to be an empirical method.

The only way to bridge this gap and to find a better way to apply SCS is by obtaining a better knowledge of the electrical phenomena involved. Since these phenomena can be described by the theory of electricity and volume conduction and because powerful computers and appropriate software became available, it was recognized by Coburn[11] and Rusinko *et al*[12] in the late '70s that computer modelling could be an appropriate method. In 1986 a similar modelling study was initiated by Holsheimer and Struijk.[13]

In this review the main aspects of SCS modelling are described. It is also shown that computer modelling is a useful tool to distinguish parameters relevant to SCS and that the model predicts several characteristics of SCS known from clinical practice. Finally, it is shown how computer modelling is used to design new SCS electrodes.

Computer models of SCS

When considering the electrical phenomena involved in SCS, two main aspects can be distinguished. First, the potential difference between electrode contacts during a stimulation pulse causes (ionic) current to flow from the anode to the cathode via the intermediate anatomical structures, named 'volume conductor'. The resulting 3-dimensional (3D) distribution of the electrical parameters current density and potential are determined by the geometry of the various anatomical structures composing the volume conductor and their electrical conductivities. Secondly, the stimulation-induced electrical field causes a fraction of the current to flow across nerve cell membranes, thereby eliciting local depolarization and hyperpolarization of these membranes. If a nerve fibre membrane is sufficiently depolarized, an action potential will be generated and propagated in both orthodromic and antidromic directions. The two separate aspects are represented by a volume conductor model and a nerve fibre model, respectively.

Volume conductor models

3-dimensional geometry As indicated, a volume conductor model represents the anatomical structures and related electrical conductivities and the stimulating

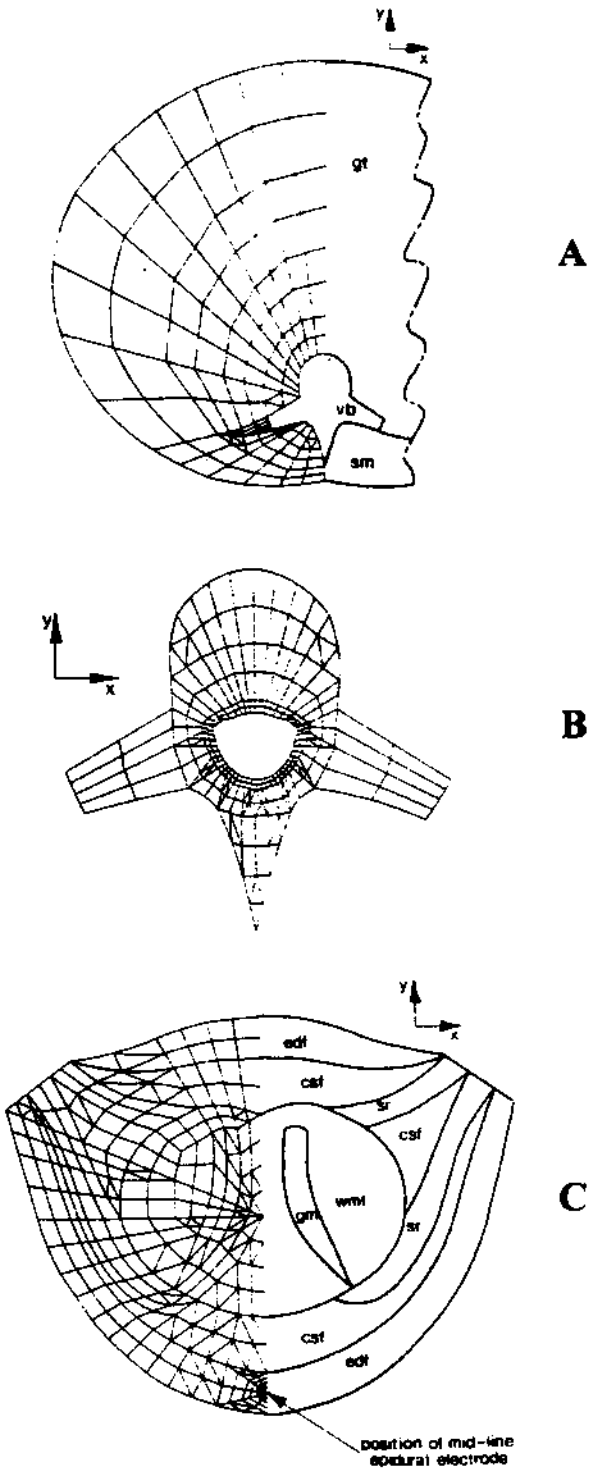

Figure 1 Transverse section of 3D finite-element model of the thorax by Coburn;[11] (**A**) complete model, (**B**) thoracic vertebra, (**C**) spinal canal; general thorax (gt), vertebral bone (vb) skeletal muscle (sm), epidural fat (edf), cerebrospinal fluid (csf), spinal root (sr), gray matter (gm), white matter (wmt)

electrode contacts. The transverse geometry of the models is based on human cadaver material,[11] computer tomographic images[11,14] and magnetic resonance images.[15] All 3D models consist of a number of layers along the spinal axis, all having the same, rather stylised transverse geometry.[14,15,17–19] Coburn[11] initially developed a transverse 2D model of the complete human thorax, as shown in Figure 1. The 2D model by Rusinko *et al.*[12] did not include the thorax and dorsal muscles. The outermost layer of their model is a bone layer of uniform thickness surrounding the spinal canal, thus contrasting the more realistically shaped vertebral bone in Coburn's model. Moreover, they inserted a dura mater layer between cerebrospinal fluid (CSF) and epidural fat. Struijk *et al*[14,15] developed 3D models with a similar transverse composition as the 2D model by Rusinko *et al.*[12] The 'surrounding' layer of their models represents all anatomical structures peripheral to the spinal canal, such as vertebral bone, dorsal muscles, thorax, fat and skin. Spinal roots are not included in their models, whereas vertebral bone and a dura mater at the dorsal side are only incorporated in later model versions,[15,19] as shown in Figure 2A.

Both Coburn's full thoracic model and the geometrically reduced models by Rusinko *et al* and Struijk *et al*[14,15] enable a reliable calculation of the potential field in the area of interest. This is due to the ratios of the electrical conductivities of these structures, as shown in Table 1. Because CSF has by far the highest conductivity, almost all current flows from the epidural contacts via the dura immediately into the CSF and little into the spinal cord (see Figure 2C). Only a few per cent flows in the epidural space, vertebral bone and intervertebral ligaments when a percutaneous electrode is used, and even less with a plate electrode. Therefore, errors in the potentials calculated in the spinal cord will be negligible when using these reduced models. Deviations from the exact geometry will presumably have a greater effect on the outcome.

3-dimensional mesh The volume conductor problem considered here, which includes inhomogenities, anisotropy and a complex geometry can not be solved analytically. Therefore, a numerical method has to be applied and the anatomical domain of interest has to be split into a mesh of volume elements which may have various shapes. Each element is defined by its conductivity and thus represents (part of) an anatomical structure. All 3D models are composed of layers along the spinal axis and each layer consists of wedges[14] or bricks[15,18,19] with a node on each corner (Figure 2A). Various shapes, including curved elements needing more nodes for their definition, can be implemented when a finite element approach is used[11,12,16,17] (Figure 1). All layers have the same architecture, except for the top and bottom ones in the models by Struijk *et al*, which are part of the 'surrounding' layer. To promote a correct calculation of the potential field, the mesh should be fine in those

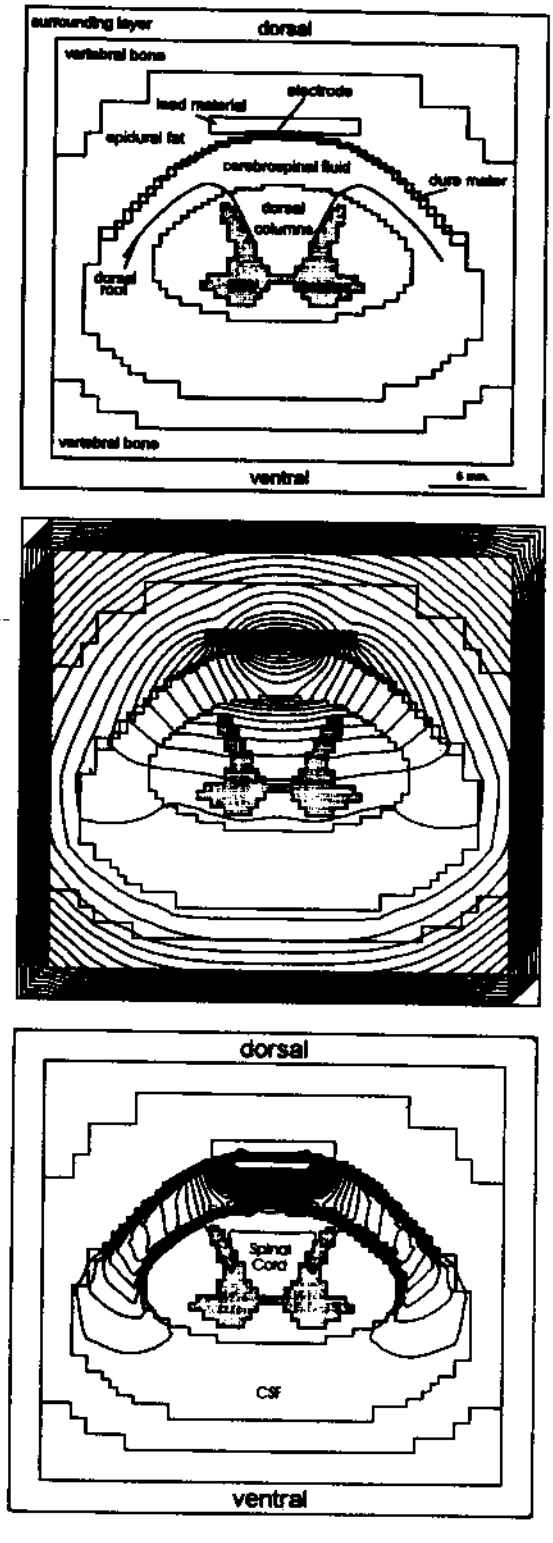

Figure 2 (A) Transverse section of cervical 3D model of the spinal canal and surrounding tissues by Struijk *et al*[15]; cathode is centred at this section, dorsal roots are not included in the model; (B) iso-potential lines in unipolar stimulation; (C) iso-current density lines in unipolar stimulation

Table 1 Tissue conductivities in $(\Omega.m)^{-1}$

	Coburn[11,16,17]	*Struijk*[14,18]	*Struijk*[15]
Gray matter	0.25	0.23	0.23
White matter transverse	0.083	0.083	0.083
longitudinal	0.72	0.60	0.60
Cerebro-spinal fluid	1.67	1.70	1.70
Spinal roots	0.15	—	—
Dura mater	–	—	0.03
Epidural fat	0.05	0.04	0.04
Vertebral bone	0.025	—	0.04
Skeletal muscle	0.105	—	—
General thorax	0.25	—	—
Surrounding layer	–	0.002	0.004 (multipolar) 0.01 (unipolar)
Electrode insulation	–	—	0.001

areas where large differences in conductivity are present and potential gradients are likely to be steep, eg, around the interface of CSF and epidural fat near the electrode contacts. A fine mesh is also preferred in those regions where nerve cell responses are calculated. Due to the limited computing capacity available in the early '80s, the complete 3D finite element model of Coburn and Sin[17] comprises only 3022 nodes. The symmetry of the model about both the midsagittal and midtransverse planes was exploited by calculating the potential field in only one quarter of the model with additional boundary conditions at these planes. The models developed some years later by Struijk *et al*[14,18] have 185 193 nodes ($57 \times 57 \times 57$) and a considerably finer mesh (smallest nodal distance 0.2 mm). Nevertheless, this model has discontinuities in eg the dorsal border of the DCs (Figure 2A), resulting in discontinuities of the potential along this border. Therefore, a finite element model as used by Coburn[11], which enables curved surfaces, should be preferred. It should be considered that the exact geometry of the models, representing a spinal length of 40–60 mm, only matters in the central part where the electrode contacts are placed and nerve cells are affected.

Coburn[11,17] implemented dorsal and ventral roots, having an approximately tenfold lower conductivity than the CSF (Table 1). Because the transverse architecture is continuous over all layers, the modelled roots introduce barriers reducing normal current flow from dorsal to lateral in the CSF (cf. Figures 1C and 2A). This effect on current density distribution in the CSF will also influence the distribution in the DCs. Considering that spinal roots split up into a number of small filaments (rootlets) embedded in CSF, Struijk *et al*[19] neglected the spinal roots in their volume conductor models. Their models are valid under the assumption that the potential distribution in the CSF surrounding the rootlets is not affected by the presence of these filaments and that the potential inside the rootlets does not differ from the potential in CSF at the same position.

Electrical conductivities The conductivities of the anatomical structures in all models have similar values, taken from the compendium by Geddes and Baker.[20] (See Table 1). All structures have an isotropic conductivity, except nerve fibre bundles and muscles. In the latter structures the conductivity parallel to the constituent fibres exceeds the value in directions normal to these fibres, as indicated for spinal white matter. Owing to their oblique orientation, Coburn[11] gave the spinal roots a single value corresponding to the mean of the longitudinal and transverse white matter resistivities. He also neglected the anisotropy of skeletal muscle in favour of a mean value and he used a mean conductivity for the main part of the thorax.

Due to the capacitance of cell membranes the conductivity of biological tissues varies with the frequency content of the electrical signal. Accordingly, tissue conductivities increase when the duration of a stimulating pulse is reduced. For rectangular pulses of 0.1–0.5 ms duration, common in SCS, the principal frequency components are 1–5 kHz. In this frequency range the transverse and longitudinal conductivities of the DCs vary approximately 23% and 3.5%, respectively.[21]

Electrode definition In all models electrode contacts are defined in the dorsal epidural space, generally next to the dura mater or CSF. Coburn and Sin[11,16,17] represented each cathode or anode by a constant current source (± 1 mA) confined to a single node of the mesh. Struijk *et al*[14,15,18,19] used electrode contacts with a rectangular shape and a realistic size, defined as constant voltage sources (1 Volt between anode and cathode). A point source is not a good electrode model, because the potential distribution in the DCs is influenced by the size of the electrode contact, especially when the distance between the contact and the spinal cord is small.[22] The current density is generally highest at the borders of a contact. Accordingly, when a realistically sized current source is used, the current has to be distributed over all contact nodes in such a way that all these nodes are at

the same voltage. This problem is avoided when voltage sources are applied.

Load resistance Coburn[11,16,17] used a constant current source in his models, because the current density in nervous tissue, and thus nerve fibre responses to stimulation are proportional to the injected current. Real SCS systems, however, deliver constant voltage pulses and, according to Ohms law, the injected current is related to both the stimulation voltage and the load resistance. To reliably model the effects of constant voltage stimulation, the load resistance of the model should have a realistic value. Struijk *et al*[15] matched their bipolar model resistance to the mean measured bipolar resistance (~1100 Ω) by inserting a dura mater layer of arbitrary thickness (0.2 mm) next to the epidural electrode contacts (having a similar size and separation as in the measurements) and giving this layer the appropriate conductivity. Because in unipolar stimulation the border of the model serves as the anode, the conductivity of the surrounding layer was adapted to match the mean measured unipolar resistance (~700 Ω), while the dura mater conductivity was the same as in bipolar stimulation. The corresponding conductivities are shown in the right column of Table 1.

Because the load resistance is measured at the pulse generator output, it includes the resistance of the biological tissues (volume conductor), the contact-tissue interfaces and the wires connecting the contacts to the pulse generator. Therefore, the calculated 'dura' resistance includes the resistances of both the dura mater, the contact-tissue interfaces and the connecting wires. The implementation of this 'dura' enables a quantitative comparison of measured and calculated perception thresholds of paraesthesia.[15] However, the contact-tissue interface has a complex impedance with a value depending on material, contact size, voltage and pulse duration (frequency content of the pulse).[23] Therefore, Struijk *et al* used the same pulse duration (210 μs) as applied in the clinical studies they used for model validation,[15] and they fitted the load impedance of the model to the value measured at the same pulse duration.

Calculation of the potential field Numerical methods applied to calculate the potentials at all nodes of a mesh are steady-state solutions, ie the boundary conditions such as voltage and current are kept constant. In both the finite element method[11,12,17] and the finite difference method[15,18,19] direct discretizations of the Laplace equation are used, resulting in second-order differences to be solved. Although these methods are basically identical, there are differences of practical interest. Finite element software packages are commercially available, whereas software for other methods is not. Moreover, the ease by which models can be assembled and modified and the time to solve the problem are different. The computing time is generally proportional to the second power of the number of nodes a model includes. As opposed to 3D models, 2D models are inappropriate for a quantitative analysis of current densities and potentials.[11,14,16]

When stimulating electrode contacts are modelled as voltage sources,[15,18,19] it should be considered that the boundary of the model is generally a voltage source as well (0 V). In unipolar stimulation this boundary is used as the anode. However, in multipolar stimulation a net current from the modelled electrode contacts to this boundary may significantly influence the voltage distribution calculated by the model. To avoid this effect, the anodal and cathodal voltages should be chosen such that the total cathodal and anodal currents are equal. This procedure is particularly needed when the numbers of cathodes and anodes or their sizes are different. When current sources are used, as in Coburn's model,[11,12,17] this problem is avoided.

Starting from an initial solution, eg all nodes of the mesh except the electrode contacts are set at 0 Volt, the nodal potentials are calculated by an iterative procedure, eg the Red-Black Gauss-Seidel optimized by a variable relaxation factor.[15] The final solution is obtained when an iteration step changes the potential field less than eg 0.01%.[15] Generally, some hundreds of iterations are needed to solve the problem. When more powerful computers became available, the initial 20 h computing time to solve Struijk's model could be reduced to 20–30 min. The number of iterations and thus computing time can be reduced another 10–20 times when a multi-level solution is applied (R Hoekema, CH Venner, JJ Struijk, J Holsheimer, paper submitted). In Figures 2B and C the distributions of potential and current density in a transverse section of a model (at the cathode level) are shown by iso-potential lines and iso-current density lines, respectively. As shown in Figure 2C, almost all current flow is in the dorsal CSF.

The computational and algorithmic correctness of the model software and the appropriateness of the spatial resolution (mesh size) can be tested by comparing the numerical and analytical solutions of simple problems (homogeneous and two compartment models).[11,14,17,19] To validate their 3D model, Coburn and Sin[17] modelled *in-situ* SCS experiments on monkeys[24] and compared calculated current densities and experimental data. However, the uncertainty regarding the exact experimental conditions prevented them from being conclusive.

Model parameter sensitivity Because most tissue conductivities are not known exactly, it is important to estimate the sensitivity of the solution to variations in tissue conductivity over normally accepted ranges. Struijk *et al*[14] calculated that the sensitivity of the potential in the DCs to variations in conductivity is highest for structures near an electrode contact (epidural fat, dura mater, CSF, DCs). Because the CSF conductivity is well known and in their model a dura mater conductivity was chosen to obtain a correct load resistance, the only relevant variables left are the longitudinal and transverse white matter conductivities.

In a recent study these conductivities were increased and reduced by a factor 2.0, which is beyond the expected range.[21] The worst case was a change in threshold stimulus of only 19% for DC fibres and 27% for dorsal root fibres (EG Olde Engberink, WA Wesselink, J Holsheimer, unpublished results).

Nerve fibre models

Electrical cable model of myelinated nerve fibre Since in 1976 McNeal[25] presented a mathematical model describing the effect of an extracellular potential field on the nodal membrane potentials of myelinated nerve fibre, this model has been applied widely. The distributed cable network model corresponds to the anatomical segmentation of the fibre. As shown in Figure 3, the nodes of Ranvier are represented by their membrane resistance and capacity, whereas the internodal axolemma is represented by its resistance. It is assumed that the myelin sheath is a perfect insulator and that geometrical relations between fibre diameter, axon diameter and internodal distance are constant. Generally, the membrane resistance is variable and includes the kinetics of ion channels underlying the generation of an action potential. McNeal[25] and Coburn[26,27] implemented the Frankenhaeuser-Huxley equations, based on the membrane kinetics of amphibian myelinated nerve, and Struijk *et al*[18,19] used the Chiu equations, derived from measurements on rabbit myelinated nerve. In both models excitation results from a large, transient increase of the Na^+ permeability. Whereas in the non-mammalian nerve fibre the membrane is repolarized mainly by an increased K^+ efflux, repolarisation in mammalian fibres occurs primarily by the 'leakage' current which is larger than in non-mammals. The implementation of these membrane kinetics enables for example modelling of the effect of stimulus pulse shape and duration. A fibre model should be sufficiently long to avoid end effects in the region of interest.[25–27] The fibre length is defined by the number of nodes and the internodal lengths, which are taken 100 times the fibre diameter.

When the positions of the nodes of a nerve fibre model in a volume conductor model are defined, the corresponding voltages are taken from the 3D potential distribution and applied to the fibre model for a limited (pulse) duration. The nodal membrane potentials are calculated according to McNeal.[25] The second-order difference of (nodal) field potentials, the 'activating function',[28] gives a qualitative indication of the effect on the corresponding nodal membrane potentials. The highest and lowest (negative) values correspond to the largest nodal depolarization and hyperpolarization, respectively. From the McNeal model it follows that a membrane is depolarised near a cathode and hyperpolarized near an anode, which is in accordance with experimental observations.[29]

The threshold stimulus to excite a nerve fibre increases with both an increasing distance from the cathode and a reduction of its calibre.[18,26,29] Therefore, large diameter nerve fibres near a cathode will generally need the lowest stimulus amplitude for their activation. In SCS such fibres are present in the superficial (dorsal) region of the DCs and in those dorsal rootlets corresponding with the rostrocaudal level of the cathode.[13,18,19,30] Therefore, and owing to their role in chronic pain management,[5] modelling of nerve fibre responses in SCS is generally limited to large diameter DC fibres and dorsal root (DR) fibres, although other target neurons have been proposed as well. It is assumed that threshold stimuli of the largest fibres correspond to the perception threshold of paraesthesia in the corresponding body areas.[15,19,26]

DC and DR fibre anatomy Most primary cutaneous afferents, upon entering the lateral part of the DCs via the dorsal root entry zone (DREZ), bifurcate into an ascending and a descending DC fibre and issue collateral branches into the spinal gray matter of primarily several segments near the DREZ.[31] Most fibres leave the DCs within several segments from the entrance zone of the corresponding dorsal root and only a fraction actually reaches the dorsal column nuclei.[32] As a result, DC fibres are gradually displaced medially while ascending and their diameter is reduced due to collateral branching.[8,32] Accordingly, fibres in the lateral DCs would have a larger calibre than in the medial part. This expectation is confirmed by the results of a morphometric study of the human T10 segment, showing a 12% reduction of the mean diameter of DC fibres larger than 7 μm from lateral to medial (HKP Feirabend, H Choufoer, J Holsheimer, unpublished results).

Characteristics of DC fibre models Coburn[26] implemented rostrocaudally directed DC fibre models with 19 nodes of Ranvier, both passive (linear) ones, having a constant membrane resistance at all nodes, and

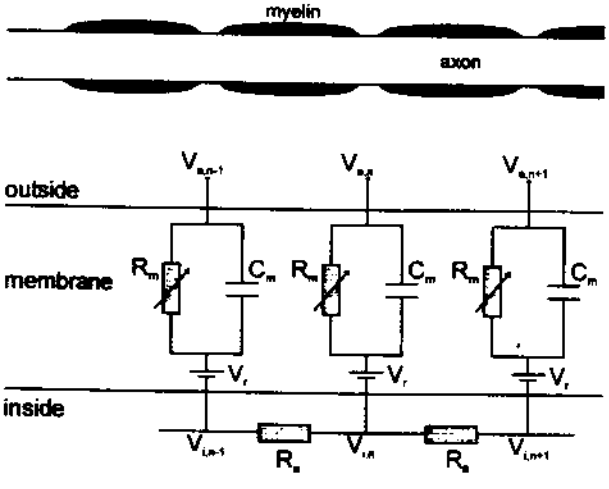

Figure 3 Distributed cable network model of myelinated nerve fibre; nodal membrane capacity (C_m), (variable) nodal membrane resistance (R_m), internodal resistance (R_a), nodal field potential (V_e), nodal intra-axonal potential (V_i) membrane resting potential (V_r)

models with excitable nodes. He showed the inverse relations of the threshold current for the excitation of fibres and their diameter and distance from the electrode, respectively. Coburn and Sin extended their linear fibre model to include collaterals attached to nodes of the main fibre and having the same diameter.[22] With a cathode at the same transverse level as a collateral, the calculated threshold current to excite the DC fibre was significantly reduced. Struijk *et al*[18] analysed the effect of collateral branching in more detail, using unipolar (cathodal) stimulation of a 6 μm diameter DC fibre model with collaterals perpendicular to the DC fibre in a ventral direction and having 81 and 20 excitable nodes, respectively. The threshold voltage was reduced by 30–40% when a single collateral of 2 μm diameter (1/3 of the DC fibre diameter) was attached in the transverse plane of the cathode and by 40–50% when multiple collaterals were present near the cathode level. It was also calculated that this threshold reduction is enhanced when the collateral has a larger diameter and when the distance between the DC fibre and the cathode is increased. Accordingly, the threshold stimulus is about proportional to the third and the second-power of the dorso-ventral fibre-to-electrode distance for a simple DC fibre and a DC fibre with one or more collaterals, respectively.[18] In contrast, threshold changes calculated for DC fibre models, both with and without collaterals, were less than 6% when the DC fibre was displaced from the spinal midline to a 2.2 mm lateral position. Therefore, the threshold stimulus of a fibre near the DC border is influenced more by its diameter than by its mediolateral position, except when the electrode is close to the DCs.[19] The proportion by which threshold stimuli of smaller diameter DC fibres rise with increasing fibre-to-electrode distance exceeds those of larger fibres.[22,30]

Coburn *et al*[33] and Struijk *et al*[18] have also shown that the depolarization of a DC fibre model in a cathodal field is accompanied by a hyperpolarization of nodal membranes of the attached collaterals. Due to the high blocking threshold, however, any propagation block of action potentials is unlikely to occur.[18]

Characteristics of DR fibre models Coburn[26] modelled DR fibres of 2.5 μm diameter and trajectories in the transverse plane with different curvatures. With the epidural cathode in the same transverse plane at midline, the calculated threshold stimuli were less than those of 5 μm DC fibres. Coburn showed that the low thresholds were most probably caused by the curvature of the DR fibre trajectories. Struijk *et al*[19] modelled DR fibres of 8 μm diameter with various curvatures, in both the transverse and the sagittal plane. They calculated that the threshold stimulus for their excitation was lowest when the cathode was centred at the transverse plane where the DR fibre enters the spinal cord, and that the initial excitation of the fibre model occurred at the node nearest to the spinal cord boundary. The low threshold at this node is primarily caused by the 20-fold reduction in electrical conductivity of the medium surrounding the DR fibre at its entrance into the spinal cord (see Table 1), resulting in a high value of the 'activating function'. This function is highest, and results in the lowest threshold, when the DR fibre enters the spinal cord perpendicularly. When its trajectory in the DREZ has a different angle in either the transverse or sagittal plane, DR fibre models have somewhat higher thresholds.[19] When varying the distance of the lowest threshold node to the spinal cord border, a threshold variation of 23% was calculated. Like Coburn,[26] Struijk *et al*[19] have shown the (additional) effect of DR fibre curvature on the threshold stimulus, presumably resulting in slightly different thresholds for fibres of the same calibre in different rootlets. A considerable effect of the change in conductivity along the DR fibre is unlikely in Coburn's model, because this model has only a twofold change in conductivity from DR to spinal cord (Table 1). The calculated threshold to excite a DR fibre near an anode was almost three times higher than near a cathode.[19,26]

Struijk *et al*[19] compared the threshold stimuli of an 8 μm DR fibre and a 6.4 μm DC fibre with collaterals at the median border of the DCs. The fibre diameter ratio was based on the conduction velocity ratio measured in man.[34] When stimulating bipolarly (10 mm centre separation), it was calculated that for an electrode-spinal cord distance less than 1.5–2 mm the DC fibre has a somewhat lower threshold than the DR fibre. However, the DC fibre threshold rises steeper than the DR fibre threshold when this distance is increased.[19,35] Due to the rostrocaudal asymmetry of the DR fibre trajectory the calculated DR fibre preference is somewhat higher when the cathode is at the rostral instead of the caudal side, although this preference is highest in unipolar stimulation.

Conclusions from SCS modelling

Neural elements stimulated by SCS

Basically, any neural element in the spinal cord can be affected by SCS if the stimulus amplitude is sufficiently high. In practice, there is only a small 'therapeutic range' of stimulation amplitudes, generally between the perception threshold of paraesthesia and a 40–60% higher voltage.[36,37] Accordingly, neural elements may be activated only if the corresponding threshold stimuli do not exceed 140–160% of the lowest threshold among DR and DC fibres. Such target elements will generally be located in the DRs and in the outer 0.2–0.3 mm of the dorsal and dorsolateral spinal cord.[30] Anodal excitation and propagation block of DC and DR fibres are highly unlikely, because the corresponding threshold voltages are about three times higher than the cathodal excitation threshold.

Apart from cutaneous DC and DR fibres, various target elements have been proposed in the literature.

Large *proprioceptive DR fibres* (only few are present in the fasciculus gracilis[32]) are most likely activated in the DREZ and elicit segmental motor effects.[7,38,39] *Ventral root (motor) fibres* are not activated in SCS.[38] Model calculations predict that the stimulus amplitude to excite a ventral root fibre exceeds the value of a DR fibre of the same calibre 14 times (WA Wesselink, J Holsheimer, unpublished results). The *dorsal spinocerebellar tract* comprises significantly larger fibres (up to 18 μm) than the DCs.[40] These fibres are likely to be activated[30] and may be involved in some effects of SCS on motor disorders. The *lateral corticospinal tract* is unlikely to be activated in SCS, because this tract is too deep in the spinal cord. Coburn[26] calculated that the threshold stimulus of a 5 μm pyramidal tract fibre is almost four times the value of a 2.5 μm DR fibre. Stimulation of *ventral spinothalamic tract* fibres giving pain relief without paraesthesia is only likely when stimulation is given by a cathode placed ventromedially.[41,42] Little is known about the effect of SCS on the *dorsal horn*. Experimental stimulation studies on spinal and neocortical gray matter have shown that the target elements are axons (primarily presynaptic axonal branches), but not cell bodies and dendrites.[43-45] Because large afferents entering the dorsal horn are most probably activated near their entrance into the spinal cord, direct activation of dorsal horn elements seems to be unlikely. From a recent SCS study by North *et al*[46] it is likely that nerve fibres in the *ligamentum flavum* contribute to nonradiating discomfort sensations if a percutaneous electrode is used. Contrary to plate electrodes, these electrodes enable current flow dorsally in the epidural space and in the *ligamentum flavum*.

Characteristics of clinical SCS

From the description of the characteristics of both volume conductor models and nerve fibre models and from additional modelling studies, various aspects of the clinical performance of SCS can be predicted. In this section model predictions relevant to the application of SCS are summarized and compared with empirical SCS data. For such a comparison the assumption was made that the perception threshold of paraesthesia is identical to the lowest of the calculated threshold stimuli of DC and DR fibres.

The most striking factor affecting the electrical field in the spinal cord, and therefore the stimulation voltage needed for paraesthesia, is the distance between the epidural electrode and the spinal cord, which is generally identical to the thickness of the CSF layer in-between.[14,16,22,35] A large intra-subject variability (among spine levels) and inter-subject variability of this layer has been shown,[47] the lowest and highest mean values being in the lower cervical and the midthoracic regions, respectively. The variations of calculated and measured paraesthesia thresholds were correlated,[15,48,49] thus supporting the prediction that the variation of paraesthesia thresholds can be attributed mainly to the variability of the dorsal CSF layer thickness. However, calculated thresholds exceeded mean perception thresholds in patients with electrodes at corresponding spine levels by a factor 2.5–3.0.[15] This discrepancy can be attributed mainly to two factors. First, the thickness of the dorsal CSF layer was based on data from normal subjects.[47] The insertion of an SCS electrode in the narrow epidural space will indent the dura, thus reducing the CSF layer thickness by 1–2 mm, which would result in a reduction of the calculated thresholds by 35–65%.[49] Secondly, thresholds were calculated with electrodes centered at the spinal cord midline, whereas the mediolateral position of SCS electrodes in patients varied from the radiological midline to 3 mm lateral, thus resulting in 10–20% lower mean values of the perception threshold.[9,15,48,49] Taking these corrections into account, the assumption that calculated threshold and perception threshold are identical is likely to be valid.

The preferential stimulation of DR fibres, resulting in initial (or exclusive) segmental paraesthesia corresponding to the cathode level, is favoured by a large dorsal CSF layer (generally in the midthoracic region), unipolar stimulation and an asymmetrical electrode position.[35,49,50] In contrast, the preferential stimulation of DC fibres, resulting in widespread paraesthesia, is favoured by a small CSF layer (lower cervical region) and bipolar or tripolar (central cathode) stimulation with neighbouring contacts centred at the spinal cord midline. These model predictions are confirmed by a multitude of empirical data.[9,10,37,39,51-55]

When in bipolar stimulation the centre separation of the cathode and the anode is 9 mm or more (as in most SCS electrodes), the stimulation is virtually unipolar.[11,22] In contrast to the cathodal position, variation of the mediolateral position of the anode has, therefore, only little effect on the paraesthesia distribution.[15] This model prediction is in accordance with empirical data.[9]

Electrode design by SCS modelling

Optimization of SCS electrode geometry

A complete coverage of the painful area by the topography of stimulation-induced paraesthesia is necessary for a successful treatment of pain,[1-3] but is difficult to obtain in many cases, especially when patients have a complex pain topography. Both empirical results and computer modelling data indicate that the activation of DR fibres, eliciting motor effects and discomfort, prevents a sufficient number of DC fibres from being activated.[54] Accordingly, the strategy to improve pain management should be to extend the range of stimulation voltage between perception threshold and discomfort threshold (therapeutic range), which implies a change of the induced electrical field in such a way that the threshold for

stimulation of DC fibres is reduced in comparison to the threshold for DR fibre stimulation. Such a change, resulting in the preferential stimulation of DC fibres, can be obtained by selecting the proper configuration (uni-, bi-, tripole) and optimizing the electrode geometry.[50,54]

The effects of the size, separation and configuration of a rostro-caudal array of electrode contacts on the thresholds of DC and DR fibre stimulation have been analyzed systematically by computer modelling.[35] It was concluded that the preferential stimulation of DC fibres is favoured by tripolar (central cathode) or bipolar stimulation with contacts having small lengths and separations. However, a reduction of the contact separation is accompanied by an increase in the stimulation voltage and current needed. Therefore, the optimum geometry has been calculated, taking into account both this aspect and the preferential stimulation of DC fibres.[56] The proposed rostro-caudal 'narrow bipole' and 'narrow tripole' electrodes have contacts with a rostrocaudal dimension of about 1.5 mm and a centre separation of 3.5–4 mm. The contacts of a plate electrode should be about 4 mm wide. This electrode geometry can be applied to all spine levels where the DCs are present.

Transverse tripolar SCS electrode

An alternative approach to increase the preferential stimulation of DC fibres is to 'shield' the DRs from stimulation by placing anodes in their vicinity. Accordingly, a tripolar configuration with a central cathode, placed normal to the spinal axis, has been proposed on basis of computer modelling.[57] To take advantage of the geometrical effects as described in the previous section, the central cathode has a small rostrocaudal dimension, whereas the anodes are longer. Another important feature of the transverse tripolar electrode is that it enables steering of the electrical field from the right to the left side of the DCs. Taking advantage of the topographical representation of the dermatomes in the DCs,[8] variation of the focus of the stimulation at the DCs from right to left will change the body areas at which paraesthesia is felt by the patient. To enable electrical steering of paraesthesia, the transverse tripolar electrode should be powered by a dual channel pulse generator, providing simultaneous constant voltage pulses of variable amplitudes. The negative outputs of the two pulse generators are connected to the central cathode, whereas each positive output is connected to a different anode.

Initial results of a clinical study with the transverse tripolar system confirm its predicted performance.[58] Paraesthesia can be moved along dermatomes on either side of the body, the therapeutic range is substantially larger than for conventional SCS electrodes, and a broad paraesthesia coverage can be obtained.

Concluding remarks

Computer modelling has been shown to be a powerful tool in the analysis of the primary effects of SCS and in the synthesis of a theoretical framework of this clinical method. Most phenomena observed in SCS are predicted by the model. Moreover, it is a useful tool in the optimization of SCS electrode design. However, a model is by definition a simplification of reality and improvements are still needed to cover all relevant empirical data. So far, the model does not predict the difference in therapeutic range between bipolar stimulation with opposite polarities as described by Law,[52] unless it is assumed that either the rostral contact is closer to the spinal cord than the caudal one, or the rostral contact is centred at the spinal cord midline and the caudal one is not, or both. Another aspect to be analyzed is the effect of pulse duration on DC fibre recruitment.[51] Finally, to predict the dermatomal recruitment order of paraesthesia for a given electrode position, the diameters of the largest DC fibres corresponding to these dermatomes and their positions in the DCs have to be estimated and implemented in the SCS model.

References

1 Simpson BA. Spinal cord stimulation. *Pain Reviews* 1994; **1**: 199–230.
2 Barolat G. Current status of epidural spinal cord stimulation (Review). *Neurosurg Quart* 1995; **5**: 98–124.
3 North RB, Roark GL. Spinal cord stimulation for chronic pain (Review). *Neurosurg Clin North Am* 1995; **6**: 145–155.
4 Shealy CN, Mortimer JT, Reswick JB. Electrical inhibition of pain by stimulation of the dorsal columns: preliminary clinical report. *Anesth Analg* 1967; **46**: 489–491.
5 Melzack R, Wall PD. Pain mechanisms: a new theory. *Science* 1965; **150**: 971–978.
6 Mullett KR, Rise MT, Shatin D. Design and function of spinal cord stimulators - theoretical and developmental considerations (Review). *Pain Digest* 1992; **1**: 281–287.
7 Dimitrijevic MR, Faganel J, Sharkey PC, Sherwood AM. Study of sensation and muscle twitch responses to spinal cord stimulation. *Int Rehab Med* 1980; **2**: 76–81.
8 Smith MC, Deacon P. Topographical anatomy of the posterior columns of the spinal cord in man. The long ascending fibres. *Brain* 1984; **107**: 671–698.
9 Barolat G, Zeme S, Ketcik B. Multifactorial analysis of epidural spinal cord stimulation. *Stereotact Funct Neurosurg* 1991; **56**: 77–103.
10 Barolat G *et al*. Mapping of sensory responses to epidural stimulation of the intraspinal neural structures in man. *J Neurosurg* 1993; **78**: 233–239.
11 Coburn B. Electrical stimulation of the spinal cord: two-dimensional finite element analysis with particular reference to epidural electrodes. *Med Biol Eng Comput* 1980; **18**: 573–584.
12 Rusinko JB, Walker CF, Sepulveda NG. Finite element modeling of potentials within the human thoracic spinal cord due to applied electrical stimulation. *Proc. 3rd Ann Conf IEEE Eng in Med Biol Soc* Houston 1981 pp. 76–81.
13 Holsheimer J, Struijk JJ. Electrode combination and specificity in spinal cord stimulation. *Proc. 9th Int Symp 'Advances in External Control of Human Extremities'*. Dubrovnik, 1987, pp. 383–404.

14 Struijk JJ, Holsheimer J, van Veen BK, Boom HBK. Epidural spinal cord stimulation: calculation of field potentials with special reference to dorsal column nerve fibres. *IEEE Trans Biomed Eng* 1991; **38:** 104–110.
15 Struijk JJ *et al*. Paresthesia thresholds in spinal cord stimulation: a comparison of theoretical results with clinical data. *IEEE Trans Rehab Eng* 1993; **1:** 101–108.
16 Sin WK, Coburn B. Electrical stimulation of the spinal cord: a further analysis relating to anatomical factors and tissue properties. *Med Biol Eng Comput* 1983; **21:** 264–269.
17 Coburn B, Sin WK. A theoretical study of epidural electrical stimulation of the spinal cord - Part I: finite element analysis of stimulus fields. *IEEE Trans Biomed Eng* 1985; **32:** 971–977.
18 Struijk JJ, Holsheimer J, van der Heide GG, Boom HBK. Recruitment of dorsal column fibers in spinal cord stimulation: influence of collateral branching. *IEEE Trans Biomed Eng* 1992; **39:** 903–912.
19 Struijk JJ, Holsheimer J, Boom HBK. Excitation of dorsal root fibers in spinal cord stimulation: a theoretical study. *IEEE Trans Biomed Eng* 1993; **40:** 632–639.
20 Geddes LA, Baker LE. The specific resistance of biological material - A compendium of data for the biomedical engineer and physiologist. *Med Biol Eng* 1967; **5:** 271–293.
21 Ranck JB, BeMent SL. The specific impedance of the dorsal columns of cat: an anisotropic medium. *Exp Neurol* 1965; **11:** 451–463.
22 Holsheimer J, Struijk JJ. How do geometric factors influence epidural spinal cord stimulation? A quantitative analysis by computer modeling. *Stereotact Funct Neurosurg* 1991; **56:** 234–249.
23 Bard AJ, Faulkner LR. Electrochemical methods. fundamentals and applications. Wiley & Sons: New York 1980.
24 Swiontek TJ *et al*. Spinal cord implant studies. *IEEE Trans Biomed Eng* 1976; **23:** 307–312.
25 McNeal DR. Analysis of a model for excitation of myelinated nerve. *IEEE Trans Biomed Eng* 1976; **23:** 329–337.
26 Coburn B. A theoretical study of epidural electrical stimulation of the spinal cord - Part II: effects on long myelinated fibers. *IEEE Trans Biomed Eng* 1985; **32:** 978–986.
27 Coburn B. Neural modeling in electrical stimulation. *CRC Crit Rev Biomed Eng* 1989; **17:** 133–178.
28 Rattay F. Analysis of models for external stimulation of axons. *IEEE Trans Biomed Eng* 1986; **33:** 974–977.
29 Ranck JB. Which elements are excited in electrical stimulation of mammalian central nervous system: a review. *Brain Res* 1975; **98:** 417–440.
30 Holsheimer J, Struijk JJ, Rijkhoff NJM. Contact combinations in epidural spinal cord stimulation, a comparison by computer modeling. *Stereotact Funct Neurosurg* 1991; **56:** 220–233.
31 Fyffe REW. Afferent fibers. In: Davidoff RA (ed). *Handbook of the spinal cord, Vols. 2 & 3 - Anatomy and Physiology*. Dekker: New York, 1984, pp 79–136.
32 Horch KW, Burgess PR, Whitehorn D. Ascending collaterals of cutaneous neurons in the fasciculus gracilis of the cat. *Brain Res* 1976; **117:** 1–17.
33 Coburn B, Sedgwick EM, Sin WK. Models of myelinated nerve fibre for studies of neurostimulation. *Proc IEE Colloq Functional Electrical Stimulation, London*, 1986, p17.
34 Desmedt JE, Cheron G. Central somatosensory conduction in man: neural generators and interpeak latencies of the far field components recorded from neck and right or left scalp and ear lobes. *Electroenceph Clin Neurophysiol* 1980; **50:** 382–403.
35 Holsheimer J, Struijk JJ, Tas NR. Effects of electrode geometry and combination on nerve fibre selectivity in spinal cord stimulation. *Med Biol Eng Comput* 1995; **33:** 676–682.
36 Jobling DT, Tallis RC, Sedgwick EM, Illis LS. Electronic aspects of spinal cord stimulation in multiple sclerosis. *Med Biol Eng Comput* 1980; **18:** 48–56.
37 Law JD. Targeting a spinal stimulator to treat the 'failed ba surgery syndrome'. *Appl Neurophysiol* 1987; **50:** 437–438.
38 Bantli H, Bloedel R, Long DM, Thienprasit P. Distribution activity in spinal pathways evoked by experimental dors column stimulation. *J Neurosurgery* 1975; **42:** 290–295.
39 Hunter JP, Ashby P. Segmental effects of epidural spinal co stimulation in humans. *J Physiol* 1994; **474:** 407–419.
40 Häggqvist G. Analyse der Faserverteilung in einem Rückenma Querschnitt (Th3). *Zeitschrift mikr-anat Forschung* 1936; **39:** 1 34.
41 Larson SF *et al*. A comparison between anterior and posteri spinal implant systems. *Surg Neurol* 1975; **4:** 180–186.
42 Hoppenstein R. Electrical stimulation of the ventral and dors columns of the spinal cord for relief of chronic intractable pai preliminary report. *Surg Neurol* 1975; **4:** 187–194.
43 Gustafsson B, Jankowska E. Direct and indirect activation nerve cells by electrical pulses applied extracellularly. *J Physi* (Lond) 1976; **258:** 33–61.
44 Nowak LG, Bullier J. Axons, but not cell bodies, are activated b electrical stimulation in cortical gray matter. I. Evidence fro chronaxie measurements. *Exp Brain Res* 1998; **118:** 477–488.
45 Nowak LG, Bullier J. Axons, but not cell bodies, are activated b electrical stimulation in cortical gray matter. II. Evidence fro selective inactivation of cell bodies and axon initial segment *Exp Brain Res* 1998; **118:** 489–500.
46 North RB, Lanning A, Hessels R, Cutchis PN. Spinal cor stimulation with percutaneous and plate electrodes: side effect and quantitative comparisons. *Neurosurg focus* 1997; **2:** 1–5.
47 Holsheimer J, Den Boer JA, Struijk JJ, Rozeboom AR. MI assessment of the normal position of the spinal cord in the spina canal. *AJNR Am J Neuroradiol* 1994; **15:** 951–959.
48 He J, Barolat G, Holsheimer J, Struijk JJ. Perception threshol and electrode position for spinal cord stimulation. *Pain* 1994; 59 55–63.
49 Holsheimer J, Barolat G, Struijk JJ, He J. Significance of th spinal cord position in spinal cord stimulation. *Acta Neurochi (Suppl)* (Wien), 1995; **64:** 119–124.
50 Holsheimer J, Wesselink WA. Effect of anode-cathode config uration on paresthesia coverage in spinal cord stimulation *Neurosurgery* 1997; **41:** 654–659.
51 Krainick J-U, Thoden U, Riechert T. Spinal cord stimulation in post-amputation pain. *Surg Neurol* 1975; **4:** 167–170.
52 Law JD. Spinal stimulation: statistical superiority of monophasic stimulation of narrowly separated, longitudinal bipoles having rostral cathodes. *Appl Neurophysiol* 1983; **46:** 129–137.
53 North RB, Ewend MG, Lawton MT, Piantadosi S. Spinal cord stimulation for chronic, intractable pain: superiority of 'multi-channel' devices. *Pain* 1991; **44:** 119–130.
54 Holsheimer J. Effectiveness of spinal cord stimulation in the management of chronic pain: analysis of technical drawbacks and solutions. *Neurosurgery* 1997; **40:** 990–996.
55 Holsheimer J, Barolat G. Spinal geometry and paresthesia coverage in spinal cord stimulation. *Neuromodulation* 1998; 1 no. 3 (in press).
56 Holsheimer J, Wesselink WA. Optimum electrode geometry for spinal cord stimulation: the narrow bipole and tripole. *Med Biol Eng Comput* 1997; **35:** 493–497.
57 Struijk JJ, Holsheimer J. Transverse tripolar spinal cord stimulation: theoretical performance of a dual channel system. *Med Biol Eng Comput* 1996; **34:** 273–279.
58 Holsheimer J, Nuttin B, King GW, Wesselink WA, Gybels JM, de Sutter P. Clinical evaluation of paresthesia steering with a new system for spinal cord stimulation. *Neurosurgery* 1998; **42:** 541–547.